Cooperative Control of Mobile Sensor Networks: Adaptive Gradient Climbing in a Distributed Environment

Petter Ögren, *Member, IEEE*, Edward Fiorelli, *Member, IEEE*, and Naomi Ehrich Leonard, *Senior Member, IEEE*

***Abstract*—We present a stable control strategy for groups of vehicles to move and reconfigure cooperatively in response to a sensed, distributed environment. Each vehicle in the group serves as a mobile sensor and the vehicle network as a mobile and reconfigurable sensor array. Our control strategy decouples, in part, the cooperative management of the network formation from the network maneuvers. The underlying coordination framework uses virtual bodies and artificial potentials. We focus on gradient climbing missions in which the mobile sensor network seeks out local maxima or minima in the environmental field. The network can adapt its configuration in response to the sensed environment in order to optimize its gradient climb.**

***Index Terms*—Adaptive systems, cooperative control, gradient methods, mobile robots, multiagent systems, sensor networks.**

I. Introduction

IN THIS PAPER, we present a method and proof for stably coordinating a group of vehicles to cooperatively perform a mission that is driven by the sensed environment. Each vehicle carries only a single sensor, and yet, with cooperation, the vehicle group performs as a mobile and reconfigurable sensor network adapting its behavior in response to the measured environment.

Technological advances in communication systems and the growing ease in making small, low-power and inexpensive mobile systems now make it feasible to deploy a group of networked vehicles in a number of environments. Furthermore, network solutions offer potential advantages in performance, robustness, and versatility for sensor-driven tasks such as search, survey, exploration, and mapping.

A cooperative mobile sensor network is expected to outperform a single large vehicle with multiple sensors or a collection of independent vehicles when the objective is to climb the gradient of an environmental field [2]. The single, heavily equipped vehicle may require considerable power to operate its sensor payload, it lacks robustness to vehicle failure and it cannot adapt the configuration or resolution of the sensor array. An independent vehicle with a single sensor may need to perform costly maneuvers to effectively climb a gradient (see algorithms in [5] and [12]), for instance, wandering significantly to collect rich enough data much like the "run and tumble" behavior of flagellated bacteria [3].

A *cooperative* network of vehicles, each vehicle equipped with a single sensor, has the potential to perform efficiently, much like animal aggregations. Fish schools, for example, efficiently climb nutrient gradients to find the densest source of food. They do so using relatively simple rules at the individual level with each fish responding only to signals in a small neighborhood. Biologists have developed a number of models for the traffic rules that govern fish schools and other animal groups (see, for example, [11], [23], [25], [26], and the references therein), and these provide motivation for control synthesis. In [27], for example, flocks were simulated on the computer using rules motivated from biology.

We aim for the cooperative network to behave as an intelligent interacting array of sensors and in this regard the biology provides inspiration. We do not try, however, to perfectly mimic the biology since there may be very different constraints associated to the vehicle group as compared to an animal group. For instance, in principle we can freely adapt intervehicle spacing, whereas fish maintain a certain average spacing for needs that include reproduction and waste management.

A motivating application for this effort is the Autonomous Ocean Sampling Network II (AOSN-II) project [7] and the experiment in Monterey Bay, CA, August 2003 [15]. The long-term goal of AOSN-II is the development of a sustainable and portable, adaptive, coupled observation/modeling system. "The system will adapt deployment of mobile sensors to improve performance and optimize detection and measurement of fields and features of particular interest" [1]. In the experiment of August 2003, the theory developed in this paper was used to coordinate a group of underwater gliders in the presence of strong currents and significant communication delays [9]. Gradients in temperature fields (among others) were estimated from the glider data; these are of interest for enabling gradient climbing to locate and track features such as fronts and eddies.

Our approach to cooperative control deliberately aims to decouple, in part, the central problems of formation maintenance and maneuver management. This eases the design and analysis of the potentially complex, network behavior. At the lowest level,

Manuscript received July 21, 2003; revised April 6, 2004. Recommended by Associate Editor M. Reyhanoglu. The work of P. Ögren was supported by the Swedish Foundation for Strategic Research through its Center for Autonomous Systems at KTH. The work of E. Fiorelli and N. E. Leonard was supported in part by the Office of Naval Research under Grants N00014-02-1-0826 and N00014-02-1-0861, by the National Science Foundation under Grant CCR-9980058, and by the Air Force Office of Scientific Research under Grant F49620-01-1-0382.

P. Ögren is with the Department of Autonomous Systems, Swedish Defense Research Agency, SE-172 90 Stockholm, Sweden (e-mail: petter.ogren@foi.se).

E. Fiorelli and N. E. Leonard are with the Department of Mechanical and Aerospace Engineering, Princeton University, Princeton, NJ 08544, USA (e-mail: eddie@princeton.edu; naomi@princeton.edu).

Digital Object Identifier 10.1109/TAC.2004.832203

each individual in the group uses control forces that derive from inter-vehicle potentials similar to those used to model natural swarms [10], [20]. These provide group cohesion and help prevent collisions. The framework is based on that presented in [16]. This framework leads to distributed control designs in which each vehicle responds to its local environment. No ordering of vehicles is necessary and this provides robustness to vehicle failures or other changes in the number of operating vehicles.

To accomplish the decoupling of the formation stabilization problem from the overall performance of the network mission, we introduce to the group a *virtual body*. The virtual body is a collection of linked, moving reference points. The vehicle group moves (and reconfigures) with the virtual body by means of forces that derive from artificial potentials between the vehicles and the reference points on the virtual body. The virtual body can translate and rotate in three-dimensional space, expand and contract. The dynamics of the virtual body are designed in two steps. In one step, extending [21], we regulate the *speed* of the virtual body using a feedback formation error function to ensure stability and convergence properties of the formation. In the other step, we prescribe the *direction* of motion of the virtual body to accomplish the desired mission, e.g., adaptive gradient climbing in a distributed environment. The development of [21] concerns coordination along prespecified trajectories.

The prescription of virtual body dynamics requires some centralized computation and communication. Each vehicle in the group communicates its state and field measurements to a central computer where the updated state of the virtual body is computed. The configuration of the virtual body is communicated back to each vehicle for use in its own local (decentralized) control law. This scenario was most practical in the AOSN-II experiment because the gliders surfaced regularly and established two-way communication with the shore station.

For gradient climbing tasks, the gradient of the measured field is approximated at the virtual body's position using the (noisy) data available from all vehicles. Centralized computation is used. We present a least-squares approximation of the gradient and study the problem of the optimal formation that minimizes estimation error. We also design a Kalman filter and use measurement history to smooth out the estimate.

Our framework makes it possible to preserve symmetry when there is limited control authority in a dynamic environment. For example, in the case of underwater gliders in a strong flow field, the group can be instructed to maintain a uniform distribution as needed, but be free to spin, and possibly wiggle, with the currents.

Of equal importance are the consequences of delays, asynchronicity, and other reliability issues in communications. In [17], for example, stability of chain-like swarms is considered in the presence of sensing delays and asynchronism. We assume in this paper that the communication is synchronized and continuous (the implementation in the Monterey Bay experiment was modified to address these kinds of realities [9]). We note that centralized computation may become burdensome for large groups of vehicles, e.g., when addressing the nonconvex optimization of formations for minimization of estimation error.

Artificial potentials were introduced to robotics for obstacle avoidance and navigation [13], [29]. In the modeling of animal aggregations, forces that derive from potentials are used to define local interactions between individuals (see [23] and the references therein). In recent work along these lines, the authors of [10] and [20] investigate swarm stability under various potential function profiles. Artificial potentials have also recently been exploited to derive control laws for autonomous, multiagent, robotic systems where convergence proofs to desired configurations are explicitly provided (see, for example, [19], [16], [24], and [31]).

Translation, rotation and expansion of a group is treated in [33] using a similar notion of a virtual rigid body called a virtual structure which has dynamics dependent on a formation error function. However, the formation control laws and the dynamics of the virtual structure differ from those presented here, and an ordering of vehicles is imposed in [33].

Gradient climbing with a vehicle network is also a topic of growing interest in the literature (see, for example, [2] and [10]). In [18], gradient climbing is performed in the context of distributing vehicle networks about environmental boundaries. In [6], the authors use Voronoi diagrams and *a priori* information about an environment to design control laws for a vehicle network to optimize sensor coverage in, e.g., surveillance applications.

The paper is organized as follows. In Section II, we review the formation framework of [16] based on artificial potentials and virtual leaders. Formation motion is introduced in Section III and the partially decoupled problems of formation stabilization and mission control are described. The main theorem for formation stabilization is presented in Section IV. Adaptive gradient climbing missions are treated in Section V. We provide final remarks in Section VI. An earlier version of parts of this paper appeared in [22].

II. Artificial Potentials, Virtual Bodies and Symmetry

In this section, we describe the underlying framework for distributed formation control based on artificial potentials and a virtual body. The framework follows that presented in [16] (with some variation in notation). Each vehicle in the group is modeled as a point mass with fully actuated dynamics. Extension to underactuated systems is possible. In [14], the authors use feedback linearization to transform the dynamics of an off-axis point on a nonholonomic robot into fully actuated double integrator equations of motion.

Let the position of the ith vehicle in a group of N vehicles, with respect to an inertial frame, be given by a vector $x_i \in \mathbb{R}^3$, $i = 1, \ldots, N$ as shown in Fig. 1. The control force on the ith vehicle is given by $u_i \in \mathbb{R}^3$. The dynamics are $\ddot{x}_i = u_i$ for $i = 1, \ldots, N$.

We introduce a web of M reference points called *virtual leaders* and define the position of the lth virtual leader with respect to the inertial frame to be $b_l \in \mathbb{R}^3$, for $l = 1, \ldots, M$. Assume that the virtual leaders are linked, i.e., let them form a *virtual body*. The position vector from the origin of the inertial frame to the center of mass of the virtual body is denoted $r \in \mathbb{R}^3$, as shown in Fig. 1. In [16], the virtual leaders move

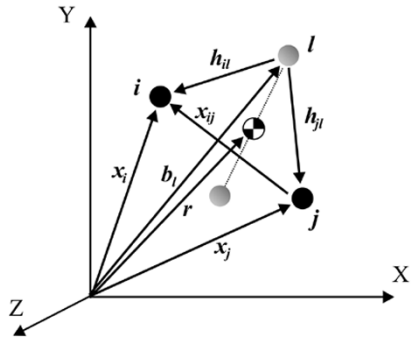

Fig. 1. Notation for framework. Solid circles are vehicles and shaded circles are virtual leaders.

with constant velocity. In this section we specialize to the case in which all virtual leaders are at rest. Motion of the virtual body will be introduced in Section III.

Let $x_{ij} = x_i - x_j \in \mathbb{R}^3$ and $h_{il} = x_i - b_l \in \mathbb{R}^3$. Between every pair of vehicles i and j we define an artificial potential $V_I(x_{ij})$ which depends on the distance between the ith and jth vehicles. Similarly, between every vehicle i and every virtual leader l we define an artificial potential $V_h(h_{il})$ which depends on the distance between the ith vehicle and lth virtual leader.

The control law u_i is defined as minus the gradient of the sum of these potentials plus a linear damping term

$$u_i = -\sum_{j\neq i}^{N} \nabla_{x_i} V_I(x_{ij}) - \sum_{l=1}^{M} \nabla_{x_i} V_h(h_{il}) - K\dot{x}_i$$
$$= -\sum_{j\neq i}^{N} \frac{f_I(x_{ij})}{\|x_{ij}\|} x_{ij} - \sum_{l=1}^{M} \frac{f_h(h_{il})}{\|h_{il}\|} h_{il} - K\dot{x}_i \quad \text{(II.1)}$$

where K is a positive–definite matrix.

We consider the form of potential V_I that yields a force that is repelling when a pair of vehicles is too close, i.e., when $\|x_{ij}\| < d_0$, attracting when the vehicles are too far, i.e., when $\|x_{ij}\| > d_0$ and zero when the vehicles are very far apart $\|x_{ij}\| \geq d_1 > d_0$, where d_0 and d_1 are constant design parameters. The potential V_h is designed similarly with possibly different design parameters h_0 and h_1 (among others), see Fig. 2.

Each vehicle uses exactly the same control law and is influenced only by near neighbor vehicles, i.e., those within a ball of radius d_1, and nearby virtual leaders, i.e., those within a ball of radius h_1. The global minimum of the sum of all the artificial potentials consists of a configuration in which neighboring vehicles are spaced a distance d_0 from one another and a distance h_0 from neighboring virtual leaders. In [16], we discuss further how to define a virtual body for certain vehicle formations. For example, the hexagonal lattice formation shown in Fig. 3 is an equilibrium for $d_0 = h_0\sqrt{3}, h_1 < d_0\sqrt{3} - h_0$, and $d_1 < d_0\sqrt{3}$.

The global minimum will exist for appropriate choice of d_1 and h_1, but it will not in general be unique. For the example of Fig. 3, the lattice is at the global minimum; however, it is not unique since there is rotational and translational symmetry of the formation and discrete symmetries (such as permutations of the vehicles). Translational symmetry of the group results because the potentials only depend upon relative distance. The

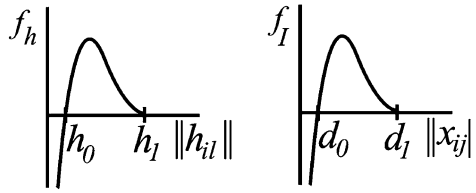

Fig. 2. Representative control forces derived from artificial potentials.

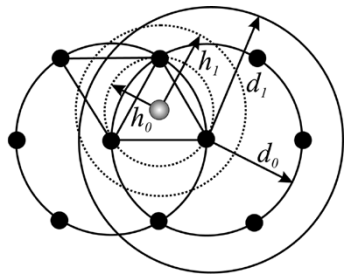

Fig. 3. Hexagonal lattice formation with ten vehicles and one virtual leader.

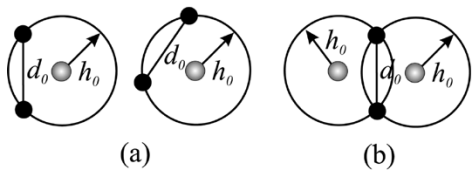

Fig. 4. Equilibrium solutions for a formation in two dimensions with two vehicles. (a) With one virtual leader there is S^1 symmetry and a family of solutions (two are shown). (b) With two virtual leaders the S^1 symmetry can be broken and the orientation of the group fixed.

rotational symmetry can, if desired, be broken with additional virtual leaders as shown in Fig. 4.

It is sometimes of interest to have the option of breaking symmetry or not. Breaking symmetry by introducing additional virtual leaders can be useful for enforcing an orientation, but it may mean increased input energy for the individual vehicles. Under certain circumstances, it may not be feasible to provide such input energy and instead more practical to settle for a group shape and spacing without a prescribed group orientation.

We define the state of the vehicle group as $x = (x_1, \ldots, x_N, \dot{x}_1, \ldots, \dot{x}_N)$. In [16], local asymptotic stability of $x = x_{\text{eq}}$ corresponding to the vehicles at rest at the global minimum of the sum of the artificial potentials is proved with the Lyapunov function

$$V(x) = \frac{1}{2}\sum_{i=1}^{N}\left(\dot{x}_i \cdot \dot{x}_i + \sum_{j\neq i}^{N} V_I(x_{ij}) + 2\sum_{l=1}^{M} V_h(h_{il})\right). \quad \text{(II.2)}$$

III. Formation Motion: Translation, Rotation, and Expansion

In this section, we introduce motion of the formation by prescribing motion of the virtual body. This motion can include translation, rotation, expansion and contraction of the virtual body and, therefore, the vehicle formation. By parameterizing the virtual body motion by the scalar variable s, we enable a decoupling of the problem of formation stabilization from the

problem of formation maneuvering and mission control. In Section IV, we prescribe the virtual body speed ds/dt which depends on a feedback of a formation error (see also [21]), and we prove convergence properties of the formation. In Section IV, we prescribe the direction of the virtual body motion, e.g., dr/ds, for gradient climbing in a distributed environment and prove convergence properties of the virtual body, and thus the vehicle network, to a maximum or minimum of the environmental field.

A. Translation and Rotation

The stability proof of [16] is invariant with respect to $SE(3)$ action on the virtual body. This simply means that the framework described in Section II is independent of the position and orientation of the virtual body. Given the positions b_l of the virtual leaders, the SE(3) action produces another set of virtual leader positions b_l'

$$b_l' = Rb_l + r, \qquad l = 1, \ldots, M$$

where $(R, r) \in (SO(3) \times \mathbb{R}^3) = SE(3)$. This action can be viewed as fixing the positions of the virtual leaders with respect to a "virtual body frame" and then moving the virtual body to any arbitrary configuration in $SE(3)$.

We exploit this symmetry by prescribing a trajectory of the virtual body in $SE(3)$, which we parameterize by s: $(R(s), r(s)) \in SE(3), \forall s \in [s_s, s_f]$ such that

$$b_l(s) = R(s)\bar{b}_l + r(s)$$

with $R(s_s)$ the 3×3 identity matrix. Here, $\bar{b}_l = b_l(s_s) - r(s_s), l = 1, \ldots, M$, is the initial position of the lth virtual leader with respect to a virtual body frame oriented as the inertial frame but with origin at the virtual body center of mass.

B. Expansion and Contraction

We similarly observe that the framework of Section II is invariant to a scaling of all distances between the virtual leaders and all distance parameters $(d_i, h_i), i = 0, 1$, by a factor $k(s) \in \mathbb{R}$. We define the configuration space of the virtual body to be $SE(3) \times \mathbb{R}$ and exploit this additional symmetry by introducing a prescribed trajectory of the virtual body in $SE(3) \times \mathbb{R}$, again parameterized by s, which now includes expansion/contraction: $(R(s), r(s), k(s)) \in SE(3) \times \mathbb{R}, \forall s \in [s_s, s_f]$ such that

$$\begin{aligned} b_l(s) &= k(s)R(s)\bar{b}_l + r(s) \\ h_i(s) &= k(s)\bar{h}_i \\ d_i(s) &= k(s)\bar{d}_i \end{aligned} \tag{III.3}$$

with $k(s_s) = 1, \bar{h}_i = h_i(s_s)$ and $\bar{d}_i = d_i(s_s)$.

C. Retained Symmetries

As discussed in Section II, it may be desirable to keep certain symmetries while controlling the formation. In the special case where the virtual body is a point mass, rotational symmetry would be preserved while translational symmetries are broken. More generally, certain symmetries can be kept by allowing the vehicles to influence the virtual leader dynamics; see [22] for details.

D. Sensor-Driven Tasks and Mission Trajectories

A third maneuver control option, distinct from prescribed trajectories and free variables, is to let translation, rotation, expansion, and contraction evolve with feedback from sensors on the vehicles to carry out a mission such as gradient climbing. This results in an augmented state–space for the system given by (x, s, r, R, k). However, it is only the directions and not the magnitude of the virtual body vector fields that we can influence since $\dot{s} = ds/dt$ is prescribed to enforce formation stability. To see this decoupling of the mission control problem from the formation stabilization problem, note that the total vector fields for the virtual body motion can be expressed as

$$\frac{dr}{dt} = \frac{dr}{ds}\dot{s}, \quad \frac{dR}{dt} = \frac{dR}{ds}\dot{s}, \quad \frac{dk}{dt} = \frac{dk}{ds}\dot{s}.$$

The prescription of $\dot{s}$, given in Section IV, controls the speed of the virtual body in order to guarantee formation stability and convergence properties. For the mission control problem Section V, we design the directions $dR/ds, dr/ds$, and dk/ds.

IV. Speed of Traversal and Formation Stabilization

We now explore how fast the system can move along a trajectory while remaining inside some user defined subset of the region of attraction. In Theorem 4.1, we prove that the virtual body traversing the trajectory $r(s), R(s), k(s)$ from $s = s_s$ to $s = s_f$ with speed prescribed by (IV.4) will guarantee the formation to converge to the final destination while always remaining inside the region of attraction, formulated as an upper bound V_U on the Lyapunov function $V(x, s)$. Here, we will be interested in the Lyapunov function $V(x, s)$, [21], that extends the Lyapunov function $V(x)$ given by (II.2) where b_l, d_i and h_i are replaced with $b_l(s), d_i(s)$ and $h_i(s)$ according to (III.3).

A. Convergence and Boundedness

Theorem 4.1 (Convergence and Boundedness): Let $V(x, s)$ be a Lyapunov function for every fixed choice of s with $V(x_{\text{eq}}(s), s) = 0$. Let V_U be a desired upper bound on the value of this Lyapunov function such that the set $\{x : V(x, s) \leq V_U\}$ is bounded. Let v_0 be a nominal desired formation speed and δ a small positive scalar. Let $h : \mathbb{R}^+ \to \mathbb{R}^+$ be a continuous function with compact support in $\{V \,|\, V \leq V_U/2\}$ and $h(0) > 0$. If the endpoint is not reached, $s < s_f$, let $\dot{s}$ be given by

$$\dot{s} = \min \left\{ v_0, h(V(x,s)) + \frac{-\left(\frac{\partial V}{\partial x}\right)^T \dot{x}}{\delta + \left|\frac{\partial V}{\partial s}\right|} \frac{(\delta + V_U)}{(\delta + V(x,s))} \right\} \tag{IV.4}$$

with initial condition $s(t_0) = s_s$. At the endpoint and beyond, $s \geq s_f$, set $\dot{s} = 0$. Then, the system is stable and asymptotically converges to $(x, s) = (x_{\text{eq}}(s_f), s_f)$. Furthermore, if at initial time $t_0, V(x(t_0), s(t_0)) \leq V_U$, then $V(x, s) \leq V_U$ for all $t \geq t_0$.

Proof: **Boundedness**: We directly have

$$\dot{V} = \left(\frac{\partial V}{\partial x}\right)^T \dot{x} + \frac{\partial V}{\partial s}\dot{s}(x, s).$$

If $(\partial V/\partial s) \leq 0$ we get $\dot{V} \leq (\partial V/\partial x)^T \dot{x} \leq 0$. If, on the other hand, $(\partial V/\partial s) > 0$, we get

$$\dot{V} \leq \left(\frac{\partial V}{\partial x}\right)^T \dot{x} + \frac{\partial V}{\partial s}\left(\frac{-\left(\frac{\partial V}{\partial x}\right)^T \dot{x}}{\delta + \left|\frac{\partial V}{\partial s}\right|}\left(\frac{\delta + V_U}{\delta + V(x,s)}\right) + h(V(x,s))\right). \quad \text{(IV.5)}$$

Now, assume that $V(x(t_0), s(t_0)) \geq V_U$. This gives

$$h(V(x,s)) = 0, \quad \frac{\delta + V_U}{\delta + V(x(t_0), s(t_0))} \leq 1, \quad \frac{\frac{\partial V(x(t_0), s(t_0))}{\partial s}}{\left(\delta + \left|\frac{\partial V(x(t_0), s(t_0))}{\partial s}\right|\right)} \leq 1$$

and $((\partial V/\partial x)^T \dot{x})(t_0) \leq 0$. Thus

$$\dot{V} \leq \left(\frac{\partial V}{\partial x}\right)^T \dot{x} + \left(\frac{-\left(\frac{\partial V}{\partial x}\right)^T \dot{x}}{1} 1 + 0\right) = 0.$$

Therefore, if $V(x,s) \geq V_U$ then $\dot{V}(x,s) \leq 0$ along trajectories in both cases. Thus, $V(x(t), s(t)) \leq V_U$ for all $t \geq t_0$ if $V(x(t_0), s(t_0)) \leq V_U$.

Asymptotic Stability: Let the extended state of the system be $(x,s) \in \mathbb{R}^n, n = 6N + 1$, and

$$\Omega_c = \{(x,s) \in \mathbb{R}^n : s \in [s_s, s_f], V(x,s) \leq V_U\}$$
$$S = \{(x,s) \in \Omega_c : \dot{s} = 0\}.$$

Since $\dot{s} \geq 0$ and $s \in [s_s, s_f]$, the limit $s_0 = \lim_{t\to\infty} s(t)$ exists. By the boundedness property of V, Ω_c is invariant and bounded. Thus, on Ω_c the ω-limit set L exists, is invariant and $(x,s) \to L \subset \Omega_c$. For $(x_L, s_L) \in L$, we must have $s_L = s_0$ and, therefore, $L \subset S$. We will now show that $\{(x_{\text{eq}}(s_f), s_f)\}$ is the largest invariant set in S and, therefore, $(x,s) \to \{(x_{\text{eq}}(s_f), s_f)\} = L$.

$\dot{s} = 0$ implies that $V(x,s)$ is a Lyapunov function with respect to x (since s is fixed). Thus, every trajectory candidate approaches $x_{\text{eq}}(s)$, where $V(x_{\text{eq}}(s), s) = 0$. This implies (by the choice of $\dot{s}$ in (IV.4)) that $\dot{s} > 0$ (due to the h term, unless $s = s_f$ where the trajectory is completed and we let s halt). Therefore, $\{(x_{\text{eq}}(s_f), s_f)\}$ is the only invariant set in S. Thus, $(x,s) \to (x_{\text{eq}}(s_f), s_f)$ and the system is asymptotically stable. ∎

Simulation of a two-vehicle planar rotation using a virtual body consisting of two virtual leaders [as shown in Fig. 4(b)] is presented in [22].

Remark 4.2: A typical choice of $h(V)$ is

$$h(V) = \begin{cases} \frac{1}{2} v_0 \left(1 + \cos\left(\pi \frac{2}{V_U} V\right)\right), & \text{if } |V| \leq \frac{V_U}{2} \\ 0, & \text{if } |V| > \frac{V_U}{2}. \end{cases}$$

Here, $h(0) = v_0 > 0$ guaranteeing asymptotic stability and giving $\dot{s} = v_0$ at $V = 0$. $\dot{s} \leq v_0$ because of the min-operator in (IV.4). Its support is limited to $|V| \leq (V_U/2)$, thus not affecting the $V \leq V_U$ property.

Remark 4.2: If the Lyapunov function V is locally positive definite and decresent and $-\dot{V}$ is locally positive definite, then one can find a class $\mathcal{K}$ function σ such that

$$\frac{-\left(\frac{\partial V}{\partial x}\right)^T \dot{x}}{\sigma(V(x,s))} \geq 1, \to \infty \text{ as } V \to 0.$$

In this case, stronger results can be proved, as in [21].

V. Gradient Climbing in a Distributed Environment

In this section, we present our strategy for enabling the vehicle group to climb (or descend) the gradient of a noisy, distributed environment. We assume that the *field is unknown* a priori, but can be measured by the vehicles along their paths. In our framework, the virtual body is directed to climb the gradient estimated from all the (noisy) measurements. The vehicles move with the virtual body to climb the gradient.

We compute a least-squares approximation of the gradient of field T using noisy measurements T_m from a single sensor per vehicle. We also study the optimal formation problem to minimize error in the gradient estimate. In the case of gradient descent, where the gradient is estimated to be ∇T_{est}, we prescribe

$$\frac{dr}{ds} = -\nabla T_{\text{est}}$$

so that the virtual body moves in the direction of steepest descent. (For gradient climbing, we use $+\nabla T_{\text{est}}$.) Using this setup and our least-squares estimate with Kalman filtering, we prove convergence to a set where the magnitude of the gradient is close to zero, thus containing all smooth local minima.

Given a computed optimal intervehicle spacing, we can also adapt the resolution of our group to best sort out the signal from the noise. For instance, one would expect to want a tighter formation, for increased measurement resolution, where the scalar field T varies greatly. Given a desired intervehicle distance Δ_d, we could let $k(s)$ evolve according to $(dk/ds) = -a(k\bar{d}_0 - \Delta_d)$, with $a > 0$ a scalar constant and $\bar{d}_0$ the initial inter-vehicle equilibrium distance, see Fig. 2. The Δ_d can be taken either from the closed-form analysis in Lemma 5.3 or from a numerical solution of the optimization problem (V.7) in Lemma 5.2.

We describe an alternate approach to gradient estimation using the gradient of the average value of the field contained within a closed region. As shown in [32], this average can be expressed as a function of the field values along only the boundary of the closed region. We present a case in which this approach is equivalent to the least-squares approach; this elucidates when we can view the least-squares estimate as an averaging process.

A. Least Squares and Optimal Distances

Fix a coordinate frame to the formation at the center of mass r of the virtual body depicted in Fig. 1, and let the position of the ith vehicle be the vector $p_i \in \mathbb{R}^l, l = 2$ or 3, in this frame. Given is a set of measurements $y = \{T_m(p_1) \ldots T_m(p_N)\}$ where $T_m(p_i)$ is a single, possibly noisy measurement, taken

by the ith vehicle at its current position p_i. We seek to estimate $x_T = (\nabla T(0)^T, T(0))^T$, i.e., the true gradient and value at $z = 0$ of the scalar field $T(z), z \in \mathbb{R}^l$. (Note that x_T here is completely different from the x used above to represent the vehicle group state.) To find the estimate we make an affine approximation $a^T z + b \approx T(z)$ of the field, and then use $(a^T, b)^T \approx x_T$. We calculate a and b using a least-squares formula and call the estimate $x_{T\,\mathrm{LS}}$.

Lemma 5.1 (Least-Squares Estimate): The best, in a least-squares sense, approximation $a^T z + b$ of a continuously differentiable scalar field $T(z)$ from a set of measurements $y = \{T_m(p_1) \dots T_m(p_N)\}$ at positions $p_i \in \mathbb{R}^l, N \geq l+1$ is given by

$$x_{T\,\mathrm{LS}} = (C^T C)^{-1} C^T y, \qquad C = \begin{bmatrix} p_1^T & 1 \\ \vdots & \vdots \\ p_N^T & 1 \end{bmatrix}.$$

It is assumed that the p_i's are such that C has full rank. Furthermore, the error due to second-order terms and measurement noise can be written

$$(x_T - x_{T\,\mathrm{LS}}) = -(C^T C)^{-1} C^T \epsilon'_E$$
$$\text{where } \epsilon'_E = \begin{pmatrix} \vdots \\ \frac{1}{2} p_i^T T''(0) p_i \\ \vdots \end{pmatrix} + \begin{pmatrix} \vdots \\ \epsilon'_{Mi} \\ \vdots \end{pmatrix}$$

ϵ'_{Mi} is measurement noise and $T''(0)$ is the Hessian of the field.

Proof: A Taylor expansion around the origin together with an assumed measurement noise ϵ'_{Mi} at each point gives the measured quantity

$$T_m(p_i) = T(0) + p_i^T \nabla T(0) + \frac{1}{2} p_i^T T''(0) p_i + \mathcal{O}(\|p_i\|^3) + \epsilon'_{Mi}.$$

Ignoring the higher order terms and writing the equations in matrix form we get $y = Cx_T + \epsilon'_E$. Applying the least squares estimate [30], minimizing $\|Cx_{T\,\mathrm{LS}} - y\|^2$, we get $x_{T\,\mathrm{LS}} = (C^T C)^{-1} C^T y$ yielding the estimation error

$$\begin{aligned}(x_T - x_{T\,\mathrm{LS}}) &= x_T - (C^T C)^{-1} C^T (C x_T + \epsilon'_E) \\ &= -(C^T C)^{-1} C^T \epsilon'_E.\end{aligned}$$

■

Remark 5.1: Note that if the measurements $T_m(p_i)$ are to be useful for estimating $\nabla T(0)$, then the distances $\|p_i\|$ must be small enough to make the lower order terms in the Taylor expansion dominate.

To formulate the optimal formation problem, we move to a stochastic framework and define the stochastic variables $\epsilon_{Mi}, i = 1, \dots, N$, and ϵ_E corresponding to the deterministic ϵ'_{Mi} (measurement error) and ϵ'_E (combined measurement and higher order terms error). Let $\epsilon_{Mi} \in N(0, \sigma_M)$, i.e., ϵ_{Mi} is Gaussian with zero mean and variance σ_M. Since the second derivative of the field in general is unknown and hard to estimate well (from noisy measurements), we replace it with a stochastic scalar variable times a matrix, $\epsilon_{Hi} H$, where $\epsilon_{Hi} \in N(0, \sigma_H)$ and H is a very rough estimate of the Hessian $T''(0)$. We let ϵ_E be a function of ϵ_{Mi} and ϵ_{Hi}.

Lemma 5.2 (Optimal Formation Problem): View the estimate error as a stochastic variable

$$(x_T - x_{T\,\mathrm{LS}}) = (C^T C)^{-1} C^T \epsilon_E$$
$$\epsilon_E = \begin{pmatrix} \vdots \\ \frac{1}{2} p_i^T H p_i \epsilon_{Hi} \\ \vdots \end{pmatrix} + \begin{pmatrix} \vdots \\ \epsilon_{Mi} \\ \vdots \end{pmatrix}.$$

Let $K(p_1, \dots, p_N) = C(C^T C)^{-1}(C^T C)^{-1} C^T$, where C depends on p_i as in Lemma 5.1. The expected value of the square error norm is

$$\begin{aligned}&E[(x_T - x_{T\,\mathrm{LS}})^T (x_T - x_{T\,\mathrm{LS}})] \\ &\quad = \sum_{i=1}^{N} \left(\frac{1}{2} p_i^T H p_i \right)^2 K(p_1, \dots, p_N)_{(i,i)} \sigma_H^2 \\ &\qquad + \mathrm{trace}(K(p_1, \dots, p_N)) \sigma_M^2. \end{aligned} \tag{V.6}$$

An optimal formation geometry problem can now be formulated as

$$\begin{aligned}&\min_{p_1, \dots, p_N} g(p_1, \dots, p_N) \\ &\qquad := \min_{p_1, \dots, p_N} E[(x_T - x_{T\,\mathrm{LS}})^T (x_T - x_{T\,\mathrm{LS}})]. \end{aligned} \tag{V.7}$$

Proof: From Lemma 5.1, we directly have

$$\begin{aligned}&(x_T - x_{T\,\mathrm{LS}})^T (x_T - x_{T\,\mathrm{LS}}) \\ &\qquad = \epsilon_E^T C (C^T C)^{-1} (C^T C)^{-1} C^T \epsilon_E = \epsilon_E^T K \epsilon_E.\end{aligned}$$

Further, $\epsilon_{Ei} = (1/2) p_i^T H p_i \epsilon_{Hi} + \epsilon_{Mi}$, giving

$$\begin{aligned}E[(x_T - x_{T\,\mathrm{LS}})^T (x_T - x_{T\,\mathrm{LS}})] &= E\left[\epsilon_E^T K \epsilon_E\right] \\ &= \sum_{i=1}^{N} \left(\frac{1}{2} p_i^T H p_i \right)^2 K_{(i,i)} \sigma_H^2 + \mathrm{trace}(K) \sigma_M^2\end{aligned}$$

since ϵ_{Hi} and ϵ_{Mi} are uncorrelated. ■

Remark 5.2: One can argue that $\epsilon_{Hi} = \epsilon_H, \forall i$. This gives a slightly different expression, but the numerical results are similar. ϵ_{Hi} can be argued to incorporate uncertain higher order terms. In this case, H is not so much a rough Hessian estimate as an estimate of which directions have large higher order terms in general.

Remark 5.3: If the symmetry is broken by the demands on sensing, i.e., an irregular formation shape is required, then the control law must break the symmetry as well. For example, an ordering of vehicles could be imposed and the different values of the parameters d_i, etc., communicated to the different vehicles.

The aforementioned optimization problem is nonconvex and therefore numerically nontrivial, i.e., standard algorithms only achieve local results. Examination of those results, however, reveals a clear pattern of regular polyhedra (deformed if $H \neq I$) around the origin with size dependent on σ_H and σ_M. Results for the two-dimensional case with three to eight vehicles can be found in Table I. For larger numbers of vehicles the minimization algorithm terminates in local minima different from regular polyhedra.

In the three-dimensional, four-vehicle, case we get an equilateral tetrahedron. The scaling and deformation effects of H, σ_H

TABLE I
LOCAL RESULTS FOR N VEHICLES $H = I, \sigma_H = \sigma_M = 1$

N	3	4	5	6	7	8
$g(p_{\min})$	1.910	1.432	1.146	0.955	0.818	0.716

and σ_M are investigated in closed form for a nonsymmetric special case in Lemma 5.3.

To illustrate nonconvexity of problem (V.7) we look at the local minimum corresponding to an equilateral triangle. Fixing the positions of two of the vehicles and plotting the objective function as the position of the third one is varied, we get the surface of Fig. 5. Note how the error increases when all three vehicles are aligned.

For a better understanding of σ_H, σ_M dependence, we consider a special case with restricted two-dimensional geometry and investigate the closed-form gradient approximation error and optimal distances in detail.

Lemma 5.3 (Optimal Formation: Three-Vehicle Case): In the two-dimensional case with three vehicles at $p_1 = (l_1, 0), p_2 = (0, l_2)$, and $p_3 = (0,0)$, we get the familiar, finite-difference approximation estimate

$$x_{T\,\mathrm{LS}} = \left(\frac{T_m(p_1) - T_m(p_3)}{l_1}, \frac{T_m(p_2) - T_m(p_3)}{l_2}, T_m(p_3) \right).$$

The estimation error variance is furthermore

$$\begin{aligned} g(l_1, l_2) &= E[(x_T - x_{T\,\mathrm{LS}})^T (x_T - x_{T\,\mathrm{LS}})] \\ &= \frac{1}{4}\sigma_H^2 \left(l_1^2 H_{11}^2 + l_2^2 H_{22}^2 \right) + \sigma_M^2 \left(2l_1^{-2} + 2l_2^{-2} + 1 \right) \end{aligned} \tag{V.8}$$

which is minimized by choosing

$$l_1 = \sqrt{\frac{2\sqrt{2}\sigma_M}{H_{11}\sigma_H}} \quad l_2 = \sqrt{\frac{2\sqrt{2}\sigma_M}{H_{22}\sigma_H}}. \tag{V.9}$$

Proof: For $p_1 = (l_1, 0), p_2 = (0, l_2)$, and $p_3 = (0,0)$

$$C = \begin{pmatrix} l_1 & 0 & 1 \\ 0 & l_2 & 1 \\ 0 & 0 & 1 \end{pmatrix} \quad (C^T C)^{-1} C^T = \begin{pmatrix} \frac{1}{l_1} & 0 & \frac{-1}{l_1} \\ 0 & \frac{1}{l_2} & \frac{-1}{l_2} \\ 0 & 0 & 1 \end{pmatrix}.$$

We now have

$$x_{T\,\mathrm{LS}} = (C^T C)^{-1} C^T (T_m(p_1) T_m(p_2) T_m(p_3))^T.$$

Looking at the errors, we get

$$\begin{aligned} K(p_1, p_2, p_3) &= C(C^T C)^{-1} (C^T C)^{-1} C^T \\ &= \begin{bmatrix} {l_1}^{-2} & 0 & -{l_1}^{-2} \\ 0 & {l_2}^{-2} & -{l_2}^{-2} \\ -{l_1}^{-2} & -{l_2}^{-2} & {l_1}^{-2} + {l_2}^{-2} + 1 \end{bmatrix}. \end{aligned}$$

Evaluating $E[(x_T - x_{T\,\mathrm{LS}})^T (x_T - x_{T\,\mathrm{LS}})]$ according to (V.6) gives (V.8). Setting the partial derivatives of (V.8) with respect to l_1 and l_2 to zero we get (V.9). ∎

Remark 5.4: The expressions for the optimal choice of l_1 and l_2 implies the following reasonable rule of thumb for different numbers of vehicles: when the noise, i.e., σ_M, increases then the distance between vehicles l_i should increase and when the second derivative, i.e., $H_{ii}\sigma_H$, increases then l_i should decrease.

B. Kalman Filter

To additionally improve the quality of the gradient estimates, we use a Kalman filter and thus take the time history of measurements into account. Using the simplest possible model of the time evolution of the true quantities, x_T, we get an observer driving the estimation toward the momentary least squares estimate $x_{T\,\mathrm{LS}}$.

Lemma 5.4 (Kalman Filter Estimate): Let the time evolution of the true gradient and scalar field, $x_T = (\nabla T^T \; T)^T$, and the measurements, $y = (T_m(p_1), \ldots, T_m(p_N))^T$, be given by the linear system

$$\dot{x}_T = bv \quad y = Cx_T + Dw$$

where $v \in N(0, I_{l+1})$ and w are white noise vectors, b is a scalar and C is given in Lemma 5.1.

Let
$D = [\mathrm{diag}((1/2)p_1^T H p_1 \sigma_H, \ldots, (1/2)p_N^T H p_N \sigma_H), \; I_N \sigma_M]$ so that $Dw = \epsilon_E$ and $w \in N(0, I_{2N})$. Then, the time evolution of the optimal estimate $x_{T\,\mathrm{KF}} = (\nabla T_{\mathrm{KF}}^T \; T_{\mathrm{KF}})^T$ is

$$\begin{aligned} \dot{x}_{T\,\mathrm{KF}} &= K(y - Cx_{T\,\mathrm{KF}}) \\ K &= PC^T (DD^T)^{-1} \\ P^2 &= b^2 (C^T (DD^T)^{-1} C)^{-1}. \end{aligned} \tag{V.10}$$

If, on the other hand, we use the simpler noise model $Dw = dI_N w$ where $d \in \mathbb{R}, I_N$ is the identity matrix and $w \in N(0, I_{2N})$. Then, (V.10) simplifies to

$$\dot{x}_{T\,\mathrm{KF}} = b^2 P^{-1} (x_{T\,\mathrm{LS}} - x_{T\,\mathrm{KF}}). \tag{V.11}$$

Proof: For a general linear system, $\dot{x} = Ax + Bv, y = Cx + Dw$, the steady-state Kalman filter [28] is

$$\begin{aligned} \dot{x}_{T\,\mathrm{KF}} &= Ax_{T\,\mathrm{KF}} + K(y - Cx_{T\,\mathrm{KF}}) \\ K &= PC^T (DD^T)^{-1} \\ 0 &= AP + PA^T - PC^T (DD^T)^{-1} CP + BB^T. \end{aligned}$$

Letting $A = 0$ and $B = bI$ we get (V.10). Plugging $D = dI$ into this makes

$$\begin{aligned} P\dot{x}_{T\,\mathrm{KF}} &= PK(y - Cx_{T\,\mathrm{KF}}) \\ &= PPC^T d^{-2} (y - Cx_{T\,\mathrm{KF}}) \\ &= b^2 d^2 (C^T C)^{-1} C^T d^{-2} (y - Cx_{T\,\mathrm{KF}}) \\ &= b^2 (x_{T\,\mathrm{LS}} - x_{T\,\mathrm{KF}}) \end{aligned}$$

which is equivalent to (V.11). ∎

Remark 5.5: If $D = I_N d$ the Kalman filter estimate is driven toward the momentary Least Squares estimate, $\dot{x}_{T\,\mathrm{KF}} = b^2 P^{-1} (x_{T\,\mathrm{LS}} - x_{T\,\mathrm{KF}})$. The speed of this motion is proportional to (b/d) (since $P^{-1} \propto (1/bd)$); faster if ∇T changes fast, i.e., large b, and slower if there is a lot of measurement noise, i.e., large d.

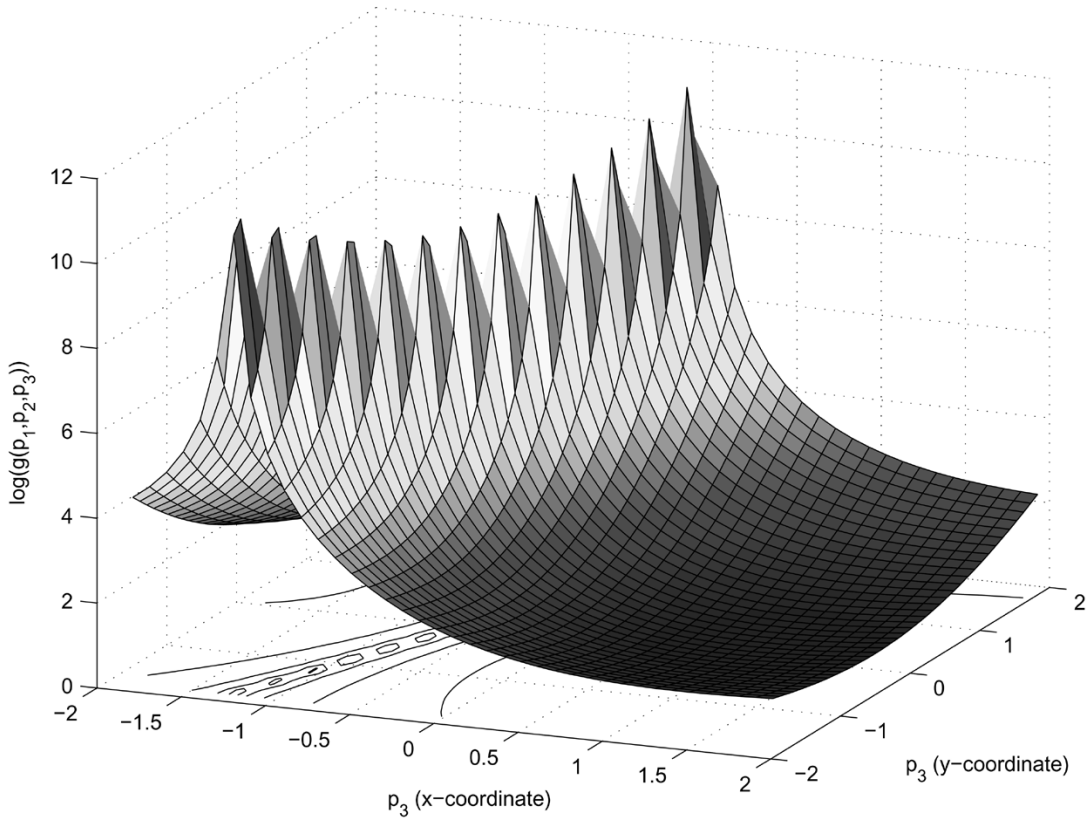

Fig. 5. Nonconvexity. The positions of two vehicles, p_1 and p_2, are fixed in the optimal triangular formation at $p_1 \approx (-0.9, -0.8)$ and $p_2 \approx (-0.2, 1.2)$, and the position of the third vehicle p_3 is varied while evaluating $g(p_1, p_2, p_3)$. Note how having p_3 close to the line through p_1 and p_2 gives a large error due to the loss of rank of $C^T C$. Due to this singularity, $\log(g)$ is plotted.

C. Convergence

To investigate how close the formation descending the gradient will get to the true local minimum in the measured field, we first translate the quantification of the estimation error back to a deterministic framework and then investigate the size of the estimation error.

Definition 5.1: Let the function $\epsilon_{\text{est}}(c, P) : \mathbb{R} \times \mathbb{R}^{(l+1)\times(l+1)} \to \mathbb{R}$ be implicitly defined by the equation

$$\int_{\|x\| \le \epsilon_{\text{est}}(c,P)} f(x)\, dx = c$$

where $f(x)$ is the probability density function [4] for $x \in N(0, \Sigma)$

$$f(x) = \det(\Sigma)^{-1/2}(2\pi)^{-l/2} e^{\frac{-1}{2}x^T \Sigma^{-1} x}.$$

The integration is in $\mathbb{R}^l$ and $\Sigma \in \mathbb{R}^{l\times l}$ is the ∇T part of the covariance matrix P, i.e.,

$$P = \begin{pmatrix} \Sigma & P_{(1\ldots l)(l+1)} \\ P_{(l+1)(1\ldots l)} & P_{(l+1)(l+1)} \end{pmatrix}.$$

Remark 5.6: Note that $\epsilon_{\text{est}}(c, P) \ge 0$ and that it is monotonically increasing in c. It also increases with a scalar resizing of P. c should be interpreted as a confidence level in the gradient estimate. For example, if one sets $c = 0.999$, then with 99.9% confidence $\|\nabla T_{\text{KF}}(r) - \nabla T(r)\| \le \epsilon_{\text{est}}(0.999, P)$.

Assumption 1 (Stochastic to Deterministic): In order to move back to a *deterministic* framework, we let the upper bound ϵ_{est} on the gradient estimation error be given by the function $\epsilon_{\text{est}}(c, P)$ defined previously in terms of the covariance matrix P and the confidence level c. That is, we assume that c has been chosen large enough so that it is reasonable to ignore the $100(1 - c)\%$ worst cases when studying the long term evolution of the dynamics. We proceed under the assumption that $\|\nabla T_{\text{KF}}(r) - \nabla T(r)\| \le \epsilon_{\text{est}}(c, P)$ *always* holds.

Theorem 5.1 (Convergence): Let the formation be given by a set of vectors $\{p_i\}$. Furthermore, use the field measurements at these points $\{T_m(p_i)\}$ to calculate an estimate ∇T_{KF}, from Lemma 5.4. If Assumption 1 holds, $T(r)$ is continuously differentiable and bounded below and the direction of motion of the virtual body is set to $(dr/ds) = -\nabla T_{\text{KF}}(r)$, then the virtual body position r will converge to a set

$$M = \{r : \|\nabla T(r)\| \le \epsilon_{\text{est}}(c, b^2(C^T(DD^T)^{-1}C)^{-1}) + \delta_M\}.$$

Here, $\sqrt{\ }$ denotes the matrix square root and δ_M is an arbitrary small positive scalar.

Remark 5.7: Since $T(\cdot)$ is continuously differentiable, the set M contains all local minima. M grows with increased noise level b and increased confidence level c. Larger δ_M also implies a larger set M but as shown later yields faster convergence to M.

Proof of Theorem: We use the notation $\epsilon_{\text{est}} = \epsilon_{\text{est}}(c, P)$, where P is calculated from $P^2 = b^2(C^T(DD^T)^{-1}C)^{-1}$. Since $(dr/ds) = -\nabla T_{\text{KF}}(r)$ we can use $V(r) = T(r)$ as a Lyapunov function. This makes

$$\dot{V}(r) = \nabla T(r)^T \frac{dr}{ds}\dot{s} = -\nabla T(r)^T \nabla T_{\text{KF}}(r)\dot{s}.$$

In Theorem 4.1 it was shown that s converges to the user defined endpoint s_f. Therefore, if we can find $k_b > 0$ such that

$$-\dot{V} \geq k_b \dot{s} \tag{V.12}$$

outside the region M and choose s_f big enough, then the trajectory must converge to M. To see this we choose $s_f = (V(r_0) - V_b)/k_b$, where V_b is a lower bound on $V(r)$ and $r_0 = r(s = 0)$. s converging to s_f now implies that V converges to V_b, (since $V \geq V_b$), or enters M where the bound is not valid. Converging to V_b however implies converging to a global minimum, which by the previous remark must be in M. Thus, we need to show that the bound (V.12) is indeed valid outside M.

Letting $E = \nabla T_{\mathrm{KF}}(r) - \nabla T(r)$ with the bound $||E|| \leq \epsilon_{\mathrm{est}}$, we get

$$\begin{aligned}\nabla T(r)^T \nabla T_{\mathrm{KF}}(r) &= \nabla T(r)^T (\nabla T(r) + E) \\ &= \|\nabla T(r)\|^2 + \nabla T(r)^T E \\ &\geq \|\nabla T(r)\|^2 - \|\nabla T(r)\|\|E\| \\ &= \|\nabla T(r)\|(\|\nabla T(r)\| - \|E\|).\end{aligned}$$

Outside of M, we get

$$\begin{aligned}\nabla T(r)^T \nabla T_{\mathrm{KF}}(r) &\geq \|\nabla T(r)\|(\|\nabla T(r)\| - \|E\|) \\ &\geq (\epsilon_{\mathrm{est}} + \delta_M)\delta_M\end{aligned}$$

implying

$$-\dot{V} \geq (\epsilon_{\mathrm{est}} + \delta_M)\delta_M \dot{s}$$

and we can choose $k_b = (\epsilon_{\mathrm{est}} + \delta_M)\delta_M$. As argued above this makes the vehicles converge to M. ∎

Remark 5.8: In this, we have assumed the p_i's to be constant. This is, however, not the case in many applications. Depending on the magnitude of the deviations one can either let them be accounted for by the sensor noise, Dw, or make the C matrix time dependent. The last option requires a nonsteady-state Kalman filter making the equations a bit longer. The P used in Assumption 1 must furthermore be replaced by an upper bound on $P(t)$.

D. Gradient-of-the-Average Approximation

Motivated by the problem of gradient climbing in a noisy environment, we examine in this subsection an alternative approach to gradient estimation: we compute the gradient of an average of the scalar environmental field values (measurements) over a closed region. This gradient is formulated as an integral over a continuous set of measurements and is approximated using the finite set of measurements provided by the vehicle group. We focus on showing that for a particular choice of discretization, i.e., numerical quadrature, and for certain distributions of vehicles over a circle in $\mathbb{R}^2$ and a sphere in $\mathbb{R}^3$, this gradient-of-the-average estimate is equivalent to the least-squares estimate. The class of vehicle formations for which this equivalence holds includes the optimal formations computed in Section V-A.

The average of a scalar field, T, inside a disc of radius h_0 is given by

$$T_{\mathrm{avg}}(r) = \frac{\int_\Omega T(x)\,dx}{\pi h_0^2}$$

where Ω is the disc of radius h_0 centered at $r \in \mathbb{R}^2$.

For a gradient climbing (or descent) problem, we seek the gradient of $T_{\mathrm{avg}}(r)$ with respect to r. In view of our disc example, we can view $\nabla_r T_{\mathrm{avg}}(r)$ as specifying the best direction to move the center of the disc so as to maximize (minimize) the average of T over Ω. As shown by Uryasev [32], this gradient can be written as

$$\nabla_r T_{\mathrm{avg}}(r) = \frac{\nabla_r \int_\Omega T(x)\,dx}{\pi h_0^2} = \frac{1}{\pi h_0^3}\int_{\partial\Omega} T(x)(x - r)\,dS$$

where $\partial\Omega$ is the boundary of Ω.

Suppose we are given only N noisy measurements T_m of T at points $x_i, i = 1, \ldots, N$, i.e., one from each vehicle. We can approximate the aforementioned integral using numerical quadrature. Consider the case in which the N vehicles are uniformly distributed over the boundary. Using the *composite trapezoidal rule*, we obtain

$$\frac{1}{\pi h_0^3}\int_{\partial\Omega} T(p + r)p\,dS \approx \frac{1}{\pi h_0^3}\sum_{i=1}^{N} T_m(p_i + r)p_i \triangle s$$

where $p = x - r, p_i = x_i - r$, i.e., the measurement location relative to r, and $\triangle s = (2\pi h_0/N)$. Changing coordinates such that the origin coincides with r

$$\nabla_r T_{\mathrm{avg}}(r) \approx \frac{2}{N h_0^2}\sum_{i=1}^{N} T_m(p_i)p_i. \tag{V.13}$$

Similarly, to compute the gradient of the average value of T within a ball of radius h_0 in $\mathbb{R}^3$, we obtain

$$\begin{aligned}\nabla_r T_{\mathrm{avg}}(r) &= \frac{3}{4\pi h_0^4}\int_{\partial\Omega} T(x)(x - r)\,dS \\ &\approx \frac{3}{N h_0^2}\sum_{i=1}^{N} T_m(p_i)p_i\end{aligned} \tag{V.14}$$

for vehicle distributions that permit N equal area partitions of the sphere with each vehicle located at a centroid of a partition, and where all vehicles do not lie on the same great circle.

Lemma 5.5 (Least Squares Equivalence): Consider N vehicles in $\mathbb{R}^l, l = 2, 3$. Suppose for $l = 2$ that the vehicles are uniformly distributed around a circle of radius h_0. Suppose in the case $l = 3$ that the vehicles are distributed over a sphere of radius h_0 such that the formation partitions the sphere into equal-area spherical polygons, where each vehicle is located at a centroid, and all vehicles do not lie on the same great circle. Denote $p_i, i = 1, \ldots, N$, the position vector of the ith vehicle relative to the center of the circle or sphere. Each vehicle takes a noisy measurement $T_m(p_i)$. Define $p^j \equiv (p_1^j, \ldots, p_N^j)^T$ where p_i^j is the jth coordinate of p_i.

Assume that the group geometry satisfies

$$\sum_{k=1}^{N} p_k^j = 0 \quad \text{and} \quad \langle p^i, p^j \rangle = \delta_{ij}\frac{N h_0^2}{l}$$

where $i, j = 1, \ldots, l$ and

$$\delta_{ij} = \begin{cases} 0, & \text{for } i \neq j \\ 1, & \text{for } i = j \end{cases}$$

and $\langle \cdot, \cdot \rangle$ is the standard inner product on $\mathbb{R}^l$. Then, the least squares gradient estimate is equivalent to the gradient-of-the-average estimate as given in (V.13) and (V.14).

Proof: A proof is only presented for formations in $\mathbb{R}^2$; the result in $\mathbb{R}^3$ follows analogously.

In terms of $p^j, j = 1, 2$

$$C^T C = \begin{pmatrix} \langle p^1, p^1 \rangle & \langle p^1, p^2 \rangle & \sum_{i=1}^N p_i^1 \\ \langle p^2, p^1 \rangle & \langle p^2, p^2 \rangle & \sum_{i=1}^N p_i^2 \\ \sum_{i=1}^N p_i^1 & \sum_{i=1}^N p_i^2 & N \end{pmatrix}.$$

It follows from the hypotheses on group geometry that $(C^T C)^{-1} = \mathrm{diag}(2/Nh_0^2, 2/Nh_0^2, 1/N)$. Furthermore

$$C^T \begin{pmatrix} \vdots \\ T_m(p_i) \\ \vdots \end{pmatrix} = \begin{pmatrix} \sum_{i=1}^N T(p_i) p_i \\ \sum_{i=1}^N T(p_i) \end{pmatrix}.$$

Thus, the least squares estimate $x_{T\,\mathrm{LS}}$ is given by

$$x_{T\,\mathrm{LS}} = \begin{pmatrix} \frac{2}{Nh_0^2} \sum_{i=1}^N T_m(p_i) p_i \\ \frac{1}{N} \sum_{i=1}^N T_m(p_i) \end{pmatrix}$$

which is equivalent to $\nabla_r T_{\mathrm{avg}}(r)$ (V.13). ■

Remark 5.9: For N vehicles in $\mathbb{R}^2$, the assumptions on the group geometry are satisfied for equally spaced vehicles on the circle. These formations are N-sided, regular polyhedra that coincide with the optimal formations for $H = \epsilon_{Hi} I$.

Remark 5.10: For vehicles in $\mathbb{R}^3$, the group geometry assumptions are not so easily satisfied; indeed, the specifications may not be achievable for arbitrary N. Examples of formations meeting the assumptions include vehicles placed at the vertices of one of the five Platonic solids, i.e., tetrahedron $(N = 4)$, octahedron $(N = 6)$, cube $(N = 8)$, icosahedron $(N = 12)$, and dodecahedron $(N = 20)$. Recall that the tetrahedron was found to be an optimal formation $H = \epsilon_{Hi} I$ in Section V-A.

Remark 5.11: When numerically integrating periodic functions, composite trapezoidal quadrature typically outperforms other methods such as the standard Simpson's Rule, high-order Newton–Cotes, and Gaussian quadratures [8]. In our numerical experiments with gradient estimation in quadratic and Gaussian temperature fields, the trapezoidal rule consistently outperformed the high-order Newton–Cotes methods by exhibiting smaller gradient estimation error. When equivalency holds, the averaging method may provide insight into when the least-squares linear approximation is appropriate for these kinds of fields.

VI. Final Remarks

We have shown how to control a mobile sensor network to perform a gradient climbing task in an unknown, noisy, distributed environment. A key result is the partial decoupling of the formation stabilization problem from the gradient climbing mission. An approach to gradient estimation and optimal formation geometry design and adaptation were presented. The latter allows for the vehicle network as sensor array to adapt its sensing resolution in order to best respond to the signal in the presence of noise. A final theorem was proved that guarantees convergence of the formation to a region containing all local minima in the environmental field. In [9], we describe application of these results to an autonomous ocean sampling glider network, including formation and gradient climbing examples and detailed simulations.

References

[1] AOSN Charter (2003). [Online]. Available: http://www.princeton.edu/~dcsl/aosn/documents/AOSN_Charter.doc

[2] R. Bachmayer and N. E. Leonard, "Vehicle networks for gradient descent in a sampled environment," in *Proc. 41st IEEE Conf. Decision Control*, 2002, pp. 113–117.

[3] H. C. Berg, *Random Walks in Biology*. Princeton, NJ: Princeton Univ. Press, 1983.

[4] P. J. Brockwell and R. A. Davis, *Time Series: Theory and Methods*, 2nd ed. New York: Springer-Verlag, 1991.

[5] E. Burian, D. Yoerger, A. Bradley, and H. Singh, "Gradient search with autonomous underwater vehicle using scalar measurements," in *Proc. IEEE OES AUV Conf.*, 1996.

[6] J. Cortés, S. Martínez, T. Karatas, and F. Bullo, "Coverage control for mobile sensing networks: Variations on a theme," in *Proc. Mediterranean Conf. Control and Automation*, Lisbon, Portugal, 2002, pp. 1–6.

[7] T. B. Curtin, J. G. Bellingham, J. Catipovic, and D. Webb, "Autonomous oceanographic sampling networks," *Oceanogr.*, vol. 6, pp. 86–94, 1989.

[8] P. J. Davis and P. Rabinowitz, *Methods of Numerical Integration*. Orlando, FL: Academic, 1984.

[9] E. Fiorelli, P. Bhatta, N. E. Leonard, and I. Shulman, "Adaptive sampling using feedback control of an autonomous underwater glider fleet," in *Proc. Symp. Unmanned Untethered Submersible Technology*, 2003, pp. 1–16.

[10] V. Gazi and K. Passino, "Stability analysis of social foraging swarms," in *Proc. 41st IEEE Conf. Decision and Control*, 2002, pp. 2848–2853.

[11] D. Grünbaum, "Schooling as a strategy for taxis in a noisy environment," *Evol. Ecol.*, vol. 12, no. 5, pp. 503–522, 1998.

[12] D. A. Hoskins, "A least action approach to collective behavior," in *Proc. SPIE, Microrobotics and Micromechanical Systems*, vol. 2593, L. E. Parker, Ed., 1995, pp. 108–120.

[13] O. Khatib, "Real time obstacle avoidance for manipulators and mobile robots," *Int. J. Robot. Res.*, vol. 5, pp. 90–99, 1986.

[14] J. Lawton, B. Young, and R. Beard, "A decentralized approach to elementary formation maneuvers," *IEEE Trans. Robot. Automat.*, vol. 19, pp. 933–941, Aug. 2003.

[15] N. Leonard and A. Robinson. (2003) *Adaptive Sampling and Forecasting Plan* [Online]. Available: http://www.princeton.edu/~dcsl/aosn/documents/ASFP.pdf

[16] N. E. Leonard and E. Fiorelli, "Virtual leaders, artificial potentials and coordinated control of groups," in *Proc. 40th IEEE Conf. Decision and Control*, 2001, pp. 2968–2973.

[17] Y. Liu, K. Passino, and M. M. Polycarpou, "Stability analysis of m-dimensional asynchronous swarms with fixed communication topology," *IEEE Trans. Automat. Contr.*, vol. 48, pp. 76–95, Jan. 2003.

[18] D. Marthaler and A. L. Bertozzi, "Tracking environmental level sets with autonomous vehicles," in *Recent Developments in Cooperative Control and Optimization*, S. Butenko, R. Murphey, and P. M. Pardalos, Eds. Norwell, MA: Kluwer, 2003.

[19] C. R. McInnes, "Potential function methods for autonomous spacecraft guidance and control," *Adv. Astronaut. Sci.*, vol. 90, pp. 2093–2109, 1996.

[20] A. Mogilner, L. Edelstein-Keshet, L. Bent, and A. Spiros, "Mutual interactions, potentials, and individual distance in a social aggregation," *J. Math. Biol.*, vol. 47, pp. 353–389, 2003.

[21] P. Ögren, M. Egerstedt, and X. Hu, "A control Lyapunov function approach to multi-agent coordination," *IEEE Trans. Robot. Automat.*, vol. 18, pp. 847–851, May 2002.

[22] P. Ögren, E. Fiorelli, and N. E. Leonard, "Formations with a mission: Stable coordination of vehicle group maneuvers," in *Proc. Symp. Mathematical Theory of Networks and Systems*, 2002, pp. 1–22.

[23] A. Okubo, "Dynamical aspects of animal grouping: Swarms, schools, flocks and herds," *Adv. Biophys.*, vol. 22, pp. 1–94, 1986.

[24] R. Olfati-Saber and R. M. Murray, "Distributed cooperative control of multiple vehicle formations using structural potential functions," in *Proc. 15th IFAC World Congr.*, 2002, pp. 1–7.

[25] J. K. Parrish and L. Edelstein-Keshet, "From individuals to emergent properties: Complexity, pattern, evolutionary trade-offs in animal aggregation," *Science*, vol. 284, pp. 99–101, Apr. 2, 1999.

[26] J. K. Parrish and W. H. Hamner, Eds., *Animal Groups in Three Dimensions*. Cambridge, U.K.: Cambridge Univ. Press, 1997.

[27] C. Reynolds, "Flocks, herds, and schools: A distributed behavioral model," in *Proc. ACM SIGGRAPH*, Anaheim, CA, 1987.

[28] I. B. Rhodes, "A tutorial introduction to estimation and filtering," *IEEE Trans. Automat. Contr.*, vol. AC-16, pp. 688–706, June 1971.

[29] E. Rimon and D. E. Koditschek, "Exact robot navigation using artificial potential functions," *IEEE Trans. Robot. Automat.*, vol. 8, pp. 501–518, Apr. 1992.
[30] G. Strang, *Linear Algebra and Its Applications*. Florence, KY: Brooks/Cole, 1988.
[31] H. Tanner, A. Jadbabaie, and G. J. Pappas, "Stable flocking of mobile agents, part I: Fixed topology," in *Proc. 42nd IEEE Conf. Decision Control*, 2003, pp. 2010–2015.
[32] S. Uryasev, "Derivatives of probability functions and some applications," *Ann. Oper. Res.*, vol. 56, pp. 287–311, 1995.
[33] B. J. Young, R. W. Beard, and J. M. Kelsey, "A control scheme for improving multi-vehicle formation maneuvers," in *Proc. Amer. Control Conf.*, 2001, pp. 704–709.

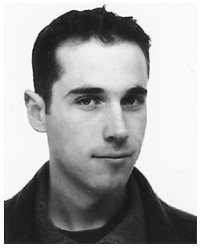

Petter Ögren (M'04) was born in Stockholm, Sweden, in 1974. He received the M.S. degree in engineering physics and the Ph.D. degree in applied mathematics from the Royal Institute of Technology (KTH), Stockholm, Sweden, in 1998 and 2003, respectively.

For four months in 2001, he visited the Mechanical and Aerospace Engineering Department, Princeton University, Princeton, NJ. He is currently working as a full-time Researcher at the Swedish Defence Research Agency (FOI). His research interests include multirobot systems, formations, navigation, and obstacle avoidance.

Edward Fiorelli (M'04) received the B.S. degree from the Cooper Union for the Advancement of Science and Art, New York, in 1997. He is currently working toward the Ph.D. degree in the Department of Mechanical and Aerospace Engineering, Princeton University, Princeton, NJ. He is currently a fifth-year graduate student in the Dynamical Control Systems Laboratory, under the direction of Dr. Naomi Leonard.

From 1997–1999, he worked as a Mechanical Engineer at Marconi Aerospace, Greenlawn, NY where he designed radar and telecommunication equipment enclosures for military aerospace applications. His research interests include multiagent control design and its application to distributed sensor networks.

Naomi Ehrich Leonard (S'90–M'95–SM'02) received the B.S.E. degree in mechanical engineering from Princeton University, Princeton, NJ, in 1985 and the M.S. and Ph.D. degrees in electrical engineering from the University of Maryland, College Park, in 1991 and 1994, respectively.

She is currently a Professor of Mechanical and Aerospace Engineering at Princeton University and an Associated Faculty Member of the Program in Applied and Computational Mathematics at Princeton. Her research focuses on the dynamics and control of mechanical systems using nonlinear and geometric methods. Current interests include underwater vehicles, mobile sensor networks, adaptive sampling with application to observing and predicting physical processes, and biological dynamics in the ocean. From 1985 to 1989, she worked as an Engineer in the electric power industry for MPR Associates, Inc., Alexandria, VA.